Characterizing larval swordfish habitat in the western tropical North Atlantic

Running title: Characterizing larval swordfish habitat

JUSTIN J. SUCA[1,2*], LEIF K. RASMUSON[1,3,4], ESTRELLA MALCA[1,3], TRIKA GERARD[3,5], JOHN T. LAMKIN[3]

1. *Cooperative Institute of Marine and Atmospheric Studies, University of Miami, 4600 Rickenbacker Causeway, Miami, FL, 33149*

2. *Biology Department, Woods Hole Oceanographic Institution, 266 Woods Hole Rd MS#33, Woods Hole, MA, 02543*

3. *Southeast Fisheries Science Center, NOAA National Marine Fisheries Service, 75 Virginia Beach Drive, Miami, FL 33149, USA*

4. *Marine Resources Program, Oregon Department of Fish and Wildlife, 2040 SE Marine Science Drive, Newport, Oregon 97376, USA*

5. University of Phoenix, South Florida Campus, 2400 SW 145 Ave, Miramar, FL 33027, USA

*Email: jsuca@whoi.edu

ABSTRACT:

Swordfish *Xiphias gladius* (Linnaeus, 1758) are a circumglobal pelagic fish targeted by multiple lucrative fisheries. Determining the distribution of swordfish larvae is important for indicating reproductive activity and understanding the early life history of swordfish. We identify and characterize larval swordfish distributions during peak swordfish spawning throughout the Gulf of Mexico and western Caribbean Sea with generalized additive models (GAMs) using catches of swordfish larvae during ichthyoplankton surveys in April and May of 2010, 2011, and 2012. The best fit GAM, as determined by stepwise, backward Akaike Information Criterion selection, included both physiochemical (temperature at 5 m, sea surface height anomaly (SSHA), eddy kinetic energy (EKE)), temporal (lunar illumination, hour of sampling) and spatial (location) variables, while near-surface chlorophyll *a* concentration residuals remained as a random effect. The highest probability of larval swordfish catch occurred at sub-surface temperatures, SSHA, and EKE values indicative of boundary currents. Standard lengths of larvae were larger further downstream in the boundary currents, despite high variability in length with location due to multiple spawning locations of swordfish near these currents. Probability of larval swordfish catch also peaked during the crescent and gibbous moons, indicating a lunar periodicity to swordfish spawning. These results suggest that swordfish may spawn during select moon phases near boundary currents that transport their larvae to larval and juvenile habitat including the northern Gulf of Mexico and coastal waters of the southeast United States.

Key Words: GAM, Larval Habitat, Gulf of Mexico, Caribbean Sea, Xiphiidae, Swordfish

INTRODUCTION:

Swordfish *Xiphias gladius* (Linnaeus, 1758) are a circumglobal oceanic fish targeted by multi-million-dollar longline and drift gill net fisheries (Ito *et al.,* 1998; Ward *et al.,* 2000). Swordfish caught in the United States Atlantic Exclusive Economic Zone (EEZ) are primarily members of the Northwest Atlantic stock as defined by the International Commission for the Conservation of Atlantic Tunas (ICCAT, 2014). Swordfish in this stock migrate from the Grand Banks off Newfoundland to the Caribbean Sea and Gulf of Mexico (Palko *et al.*, 1981; Nakamura, 1985; Neilson *et al.*, 2014). Juvenile swordfish (< 130 cm) prefer warmer waters such as the Gulf of Mexico and waters of the southeast US, while larger swordfish primarily occupy waters with colder surface temperatures, such as Georges Bank (Muhling *et al.,* 2015).

In addition to large scale geographical migrations, adult swordfish are vertical migrators, spending nights near the surface and diving to depths of ~900 m during daylight (Takahashi *et al.,* 2003; Abascal *et al.,* 2010). This behavior matches the similar vertical migration of their prey items: squid and mesopelagic fishes (Scott and Tibbo, 1968; Chancollon *et al.,* 2006). Further, the extent of vertical migration is influenced by the lunar phase with swordfish ascending to shallower (deeper) depths in low (high) lunar illumination (Lerner *et al.,* 2013).

Northwest Atlantic swordfish populations spawn year-round in the Atlantic, from Cape Hatteras to the waters North of Puerto Rico (see Fig. 1), including the Caribbean Sea and Gulf of Mexico (Arata, 1954; Grall *et al.,* 1983; Govoni *et al.*, 2000; 2003; Bremer *et al*., 2005). Most spawning occurs between December and June in the Gulf of Mexico and Caribbean (Taylor and Murphy, 1992; Arocha, 1997; Govoni *et al*., 2003). The neustonic eggs of swordfish spawned in the Caribbean Sea (where average temperatures are ~25^{o}C) take approximately three days to hatch (Yasuda *et al*., 1978; Enfield and Mayer, 1997). After hatching, pre-flexion swordfish larvae occupy the upper 10 m of the water column, exclusively consuming copepods (Govoni *et*

al., 2003). Swordfish larvae become neustonic and piscivorous at approximately two weeks of age, corresponding to notochord flexion (Govoni *et al.,* 2003).

Swordfish larvae of various sizes have been found throughout the western Atlantic and Caribbean, resulting in uncertainty in their spawning locations. Grall *et al.* (1983) observed small larvae (<10 mm) in the eastern Caribbean and Straits of Florida and larger larvae (> 10mm) near the western Antilles. Govoni *et al.,* (2000) suggested that larvae may be spawned as far north as Cape Hatteras. Further, estimations of spawning locations for swordfish larvae caught in the Gulf of Mexico and Caribbean have ranged from the north central Gulf of Mexico to the eastern Caribbean, suggesting spawning may occur as far south as the southern extent of the Sargasso Sea and the beginning of the Caribbean Current (Govoni *et al.,* 2003). Distribution and larval habitat have also been described for swordfish larvae in the north central Gulf of Mexico, suggesting that spawning may occur within the Gulf of Mexico (Rooker *et al.,* 2012). However, the spatial and temporal extent of many of these studies were limited, with either a limited intra-seasonal spatial extent or spatially limited to regions in the Gulf of Mexico or southeastern United States (Govoni *et al.,* 2000; Rooker *et al.,* 2012).

Surface transport in the Gulf of Mexico and western Caribbean Sea is dominated by the Caribbean, Yucatan, and Loop Currents, which become the Florida Current and ultimately the Gulf Stream after passing through the Straits of Florida (Fig. 1; Oey *et al.,* 2005). The Caribbean and Loop Currents flow over large zonal distances (≥ 400 km in the case of the Loop Current), permitting meanders that can separate from the dominant current in the form of mesoscale eddies (Candela *et al.,* 2002; Richardson, 2005). The Yucatan Current, however, passes through a topographically constrained channel, resulting in minimal eddy shedding and less variability in its zonal extent (Oey *et al.,* 2005; Carillo *et al.,* 2016). The fronts associated with boundaries of

the current systems, as well as the anticyclonic mesoscale eddies they shed, create convergence zones that concentrate plankton and form essential habitat for pelagic organisms (Bakun, 1996; 2006). These convergent zones in the Gulf of Mexico and Caribbean Sea are often used for spawning and larval habitat by large pelagic fishes such as Atlantic bluefin tuna *Thunnus thynnus* (Linnaeus, 1758) and sailfish *Istiophorus platypterus* (Shaw, 1792; Teo *et al.,* 2007; Richardson *et al.,* 2009; Muhling *et al.,* 2010; Simms *et al.,* 2010). Areas of convergence, such as the Gulf Stream front, serve as habitats for pre-flexion larvae because due to their ability to concentrate larval swordfish (Govoni *et al.,* 2000). Rooker *et al.,* (2012) also showed that the greatest probabilities of larval swordfish catches are associated with the Loop Current boundary, further suggesting that fronts may serve as larval swordfish habitat.

Data from ichthyoplankton surveys along with oceanographic parameters can begin to elucidate seasonal patterns of larval fish distributions (Houde *et al.,* 1979; Hernandez *et al.,* 2010; Muhling *et al.,* 2010; 2012; Domingues *et al.,* 2016). Habitat models can be formed using catch data and bio-physical data collected during surveys to predict larval fish distributions to better understand the diversity and abundance of these larvae in the pelagic environment (Rooker *et al.,* 2012). The purpose of this work was to identify and predict larval swordfish distributions during the months of April and May, encompassing part of the peak spawning for swordfish throughout the Gulf of Mexico and western Caribbean Sea (Govoni *et al.,* 2003). This provides an opportunity to assess the distribution of swordfish in this region during the same season for three consecutive years, significantly improving our current understanding of larval swordfish distribution and swordfish spawning. Based on observations of swordfish larvae in the Gulf of Mexico and Caribbean, we hypothesized that larvae will most likely to be found in the Caribbean, Yucatan, and Loop Currents which may serve to transport larvae to suitable habitat to

optimize growth and/or survival. This work assesses this hypothesis through formation of habitat models to improve our understanding of the life history of swordfish and further predicts spawning locations based on the size of larvae collected.

METHODS:

Data collected during the 2010-2012 Southeast Area Monitoring and Assessment Program (SEAMAP) Spring Ichthyoplankton Surveys were used to determine how oceanographic features influence the presence/absence of swordfish larvae. Sampling occurred during the months of April and May in the western Gulf of Mexico, the edge of the Loop Current, and the Yucatan Channel. Western Caribbean sampling regions varied by year (Fig. 2). Plankton tows were conducted at each station undulating a 1 x 2m 0.505 mm mesh net fitted with a flowmeter (2030R, General Oceanics, Inc) between the surface and 10 m depth for 10 minutes (hereafter referred to as S-10; Habtes *et al.,* 2014). Additional neuston tows were also conducted for 10 min at various stations using a 1 x 2m 0.947 mm mesh net. Tows were conducted during both day and night. Volume filtered for each tow (m^3) was calculated from flowmeter counts. At most stations a Seabird SBE 9/11 Plus CTD (conductivity, temperature, and depth) equipped with a dissolved oxygen sensor (SBE 43) was deployed to 300 m. CTD casts were restricted to 50 m above the bottom for stations shallower than 350 m.

Data Processing/Physical Variables:

Swordfish larvae were identified using morphological characteristics by the Sea Fisheries Institute, Plankton Sorting and Identification Center in Szczecin, Poland. Body length was measured as standard length (SL) or notochord length (NL) to the nearest 0.05 mm (Supp. Table 1). Maps of the presence/absence and SL of swordfish larvae for each cruise were generated

using Esri ArcGIS system (Desktop 10.4.1). Sea surface temperature data from the Hybrid Coordinate Ocean Model (HYCOM) 1/12^{o} resolution Global Reanalysis (http://hycom.org/data/glbu0pt08/expt-19pt1) were interpolated using the Marine Geospatial Ecology Toolbox across the sampling region (Roberts *et al.,* 2010).

Physicochemical parameters were obtained from in-situ CTD data, satellite data, and HYCOM for use in habitat model formation. Values for daily average sea surface height anomaly and current velocity were obtained for each station using HYCOM estimates. Eddy kinetic energy was calculated from these current velocities using the formula:

$$[1]\quad EKE = \tfrac{1}{2}(u^2+v^2)$$

where EKE represents eddy kinetic energy (m^2s^{-2}), *u* represents zonal velocity and *v* represents the meridional velocity. Near-surface chlorophyll *a* concentrations for each sampling station were approximated from the eight-day averaged and 9 km resolution Moderate Resolution Imaging Spectroradiometer (MODIS), courtesy of the NASA Goddard Space Flight Center, Ocean Ecology Laboratory, Ocean Biology Processing Group, Greenbelt, MD, USA (https://oceandata.sci.gsfc.nasa.gov/MODIS-Aqua/Mapped/8Day/9km/chlor_a). Bathymetry (0.03^{o} resolution) at each station was extracted from the NOAA Center for Environmental Information bathymetry raster (http://maps.ngdc.noaa.gov/viewers/wcs-client/). Fraction of lunar illumination for each sample day was obtained from the US Navy database (http://aa.usno.navy.mil/data/docs/MoonFraction.php).

Physicochemical parameters considered in model development were: temperature (^{o}C) at 5 m, temperature (^{o}C) at 100 m, near-surface chlorophyll *a* concentration residuals calculated by

removing the temperature trend (mg m^{-3}), dissolved oxygen (5 m) residuals calculated by removing the temperature trend (mg L^{-1}), salinity (5 m), year, hour of day, latitude, longitude, fraction of lunar illumination, depth (m), eddy kinetic energy (m^2 s^{-2}), sea surface height anomaly (m), sea surface height anomaly gradient, and eddy kinetic energy gradient (Table 1). This suite of variables was chosen because they can be used to differentiate and characterize oceanographic features in the sampling region. Volume of water filtered (m^3), hereafter volume filtered by the net was log transformed for each station and included to standardize sampling effort because of positive skew in the volume filtered values. All *in situ* variables (temperature, dissolved oxygen, and salinity) were determined as the value closest to the desired depth (5 m or 100 m) from the CTD downcast. Residuals of a linear regression with temperature of both dissolved oxygen and chlorophyll *a* were used because oxygen and chlorophyll *a* were strongly collinear with temperature ($r=-0.74$, $p<0.01$; $r=-0.49$, $p<0.01$; Fig. 3). The temperature trend was removed because it drives patterns of both dissolved oxygen and chlorophyll *a* (Garcia and Gordon, 1992; Feng *et al.,* 2015). Gradient of sea surface height anomaly and gradient of eddy kinetic energy were calculated as the gradient between the two nearest HYCOM values ($1/12^o$ separation) to each station for the day of sampling.

Stations lacking CTD casts or containing errors in oxygen values due to sensor malfunction were removed. In addition, stations sampled in continental shelf waters (<200 m depth) were removed prior to model formation (n =117 stations removed in total). This is due to high hydrographic variability in coastal waters (thus the poor accuracy of HYCOM in these regions) and previous studies suggesting that swordfish larvae are rare in depths < 200 m (Grall *et al.,* 1983; Chassignet *et al.,* 2007).

Model Formation:

The aforementioned variables were used to develop generalized additive models (GAMs) in order to explore the effects of the physical environment on the distribution of swordfish larvae (Hastie and Tibshirani, 1990). GAMs are statistical models that allow a combination of physicochemical parameters to interact in a non-linear manner with the response variable and are non-linear extensions of generalized linear models (Barry and Welsh, 2002). These models provide a means to discover larval habitats that are difficult to identify through linear models and simple correlations.

GAMs for this project were developed using the *mgcv* library in R statistical software (Version 3.2.3) (Wood, 2008; 2017). We developed presence/absence models rather than abundance (e.g. catch per unit effort) since abundance data for ichthyoplankton can be difficult to assess due to the patchy distribution of fish larvae and the course spatial scale of sampling. The response variable for all models was the presence/absence of swordfish in the S-10 tows as these were conducted at each station and showed a higher frequency of swordfish catch than the neuston net. All predictor variables were tested for covariance and collinearity using a correlation matrix followed by plotting and calculating Pearson's product-moment correlation coefficients (r) for each set of covariates. Correlation of predictor variables to the response variable were then analyzed through single variable GAMs. The predictor variable showing largest deviance explained when plotted against the response variable was selected for use in the model. Models were developed using a binomial distribution with a logit link function. Smooth functions related the response variable (larval presence/absence) to the model parameters, permitting non-linear relationships. Each smoothing function was permitted three degrees of freedom to minimize overfitting with the exception of fraction of lunar illumination, which was permitted five (Sunbland *et al.,* 2009; Rooker *et al.,* 2012). Five degrees of freedom permits the

fraction of lunar illumination to incorporate sinusoidal and bimodal responses. Response curves provided visual representations of the smooth functions to qualitatively relate patterns of presence/absence to physicochemical parameters.

Three parameters were removed due to collinearity: temperature at 100 m (collinear with temperature at 5m, r =0.62), EKE gradient (collinear with temperature at 5m, r= -0.45), and sea surface height anomaly gradient (collinear with EKE, r=0.55). After removal of these variables, the base model included eleven predictor variables and was developed using the following equation:

[2] Swordfish presence=offset(log(Volume filtered))+s(Temperature at 5 m)+s(Oxygen residuals) + s(Chlorophyll-*a* residuals) + s(Salinity at 5 m) + s(Fraction of Lunar Illumination) + s(Depth) + s(Sea Surface Height) + s(Eddy Kinetic Energy) + te(Longitude,Latitude) + s(Hour of Sampling)+Year

Where s represents a smooth function and te represents a tensor spline, which allows longitude and latitude to interact anisotropically (Zurr, 2012; Wood, 2017).

A stepwise backwards Akaike Information Criterion (AIC) method was used to select the best fit model. AIC is calculated using the following formula

[3] $AIC=-2l+2k$

where l is the maximized log likelihood and K is the number of estimable parameters (Burnham and Anderson, 2002). The model that resulted in the lowest AIC was selected for each iteration with the exception of situations where the response curves did not permit reasonable ecological inference. Model selection was further verified by examining the Akaike weights for each

iteration of models to select the best model. Akaike weights are calculated through the following equation:

$$[4]\ w_i = \frac{\exp[-\frac{1}{2}\Delta_i]}{\sum_{i=0}^{n}\exp[-\frac{1}{2}\Delta_i]}$$

Where Δ_i represents the difference in AIC of a particular model from the lowest AIC for any model in that iteration. Akaike weights can be interpreted as the probability that a model is the best model for the iteration (Burnham and Anderson, 2002).

Once a best-fit model was determined, bootstrapping was used to make a Receiver Operating Characteristic (ROC) curve and measure the area under that curve (AUC). A randomly selected subset of 120 stations was used as a training data set (approximately one quarter of the data) with the remaining data serving as the test data set (Huberty, 1994). The true positive rate of the bootstrap simulation was plotted against the false positive rate to create a ROC curve. The integration of this curve results in an AUC value. AUC values close to one represent a good fit of the model to the data set, with values exceeding 0.90 considered excellent. This bootstrapping was repeated 1000 times and the mean, median, and standard deviation of these AUC scores were calculated.

RESULTS:

One hundred and ninety-seven swordfish larvae were collected from S-10 and neuston nets over the three years of sampling with 78 of 603 (12.96%) stations sampled positive for presence of swordfish larvae (Fig. 2). Mapping of swordfish catch with monthly mean sea surface temperature showed a clear association of swordfish larvae with the waters of Caribbean Current, Yucatan Current, and Loop Current. The only exceptions were in two stations

containing swordfish larvae near the continental rise of the northwest Gulf of Mexico in 2012 (Fig. 2c)

Larger swordfish larvae (>6.5mm) were also generally caught in the Loop Current with small individuals (<6.5 mm) being more present near the Yucatan and Caribbean Currents (Fig. 4). The exception was 2012 which showed small larvae near the southeastern extent of the Loop Current as it becomes the Florida Current. There were also three stations containing large swordfish larvae near Hispaniola in 2011.No significant correlation with latitude and standard length of swordfish was found ($r=0.05$, $p=0.63$). Smaller individuals were also present in the northern and western Loop Current in 2010 and 2011 while eastern extent of the Loop Current primarily contained larger larvae in these years.

Model:

Four hundred and eighty-six stations remained (62 stations containing swordfish larvae) after oxygen outliers, stations without CTD casts, and shelf waters were removed from the dataset for model formation (Fig. 2).

Seven variables remained in the model after a backwards step-wise AIC model selection: temperature at 5 m, SSHA, EKE, fraction of lunar illumination, hour of sampling (local time), and an interaction between latitude and longitude (Table 2). Chlorophyll *a* residuals were also included as a random effect in the model as they reduced residual heterogeneity (Zurr *et al.,* 2009). This was because the smooth function of chlorophyll *a* residuals was not significant in the model, but did show collinearity when plotted against residuals of a GAM that did not include chlorophyll *a* residuals.

The final AIC for this model was 290.542 and the total deviance explained (DE) was 33.1% (Table 3). The variables in order of greatest ΔAIC were longitude and latitude (ΔAIC

=19.02, ΔDE=6.3%), percent lunar illumination (ΔAIC =17.91, ΔDE=7.7%), temperature at five meters (ΔAIC =13.65, ΔDE=9.7%), hour of sampling (ΔAIC =9.58, ΔDE=2.0%), sea surface height anomaly (ΔAIC =8.10, ΔDE=1.9%) and eddy kinetic energy (ΔAIC =2.98, ΔDE=0.1%). The Akaike weight for the model selected in the final iteration was 0.780, which was strongly indicative of the best-fit model. The ROC curve for the final model indicated a strong predictive capability of the model within the dataset. The average AUC for 1000 runs was 0.865, a median AUC of 0.866, and a standard deviation of 0.047.

Probability of swordfish presence increased as temperature increased from 24^{o}C to 28^{o}C with highest catch at surface temperatures of 28 ^{o} C (Fig. 5a). Probability of larval swordfish catch reached a maximum around 0.17 m SSHA with a near parabolic curve showing lowest probability around both low (-0.4 m) and high (0.6 m) SSHA (Fig. 5b). Probability of catch decreased as eddy kinetic energy increased, though the magnitude of additive effect was minimal (Fig. 5c). Fraction of lunar illumination displayed an uneven sinusoidal pattern with peak probability of catch occurring prior to gibbous (0.75 illumination) and crescent (0.25 illumination) moons (Fig. 5d). Lowest probability of catch occurred during the quarter-moons (0.5 illumination). The response curve for hour of collection was significant, but showed little overall effect on probability of catch. Highest probability occurred between 1000-1500 local time (Fig. 5e). No significant relationship or pattern between fraction of lunar illumination and hour of sampling occurred, indicating that these parameters had independent effects on the catch of swordfish larvae.

DISCUSSION:

This study shows a clear association between the presence of larval swordfish and the fast-moving currents in the western Caribbean Sea and Gulf of Mexico (Fig. 2). Our habitat models corroborate these findings with the highest probabilities of catching larvae at physicochemical values indicative of these current systems. Additionally, assessment of the standard length of larvae by region corroborates findings from previous catches of larval swordfish and mature adults that suggest there are likely multiple spawning locations south of the Gulf of Mexico near the Caribbean Current and Yucatan Channel, with possible spawning occurring in the northern and western extents of the Loop Current (Govoni *et al.,* 2003; Arocha, 2007; Rooker *et al.,* 2012). These concepts have been documented before but this study expands our knowledge of the physicochemical parameters that constitute larval habitat throughout both the Gulf of Mexico and Caribbean Sea, differentiates the oceanographic features likely used for spawning by swordfish, indicates a connection between lunar illumination and swordfish spawning, and documents new locations and abundances of swordfish larvae throughout the western tropical North Atlantic.

The response curve for temperature at 5 m supports this hypothesis, showing a higher additive effect with increasing temperature. This result suggests the presence of larvae in warm waters, a characteristic of the Loop Current (Domingues *et al.,* 2016). These values were consistent with Rooker *et al.,* (2012), which observed peak catch of swordfish larvae at temperatures around 28^{o} C. However, their sampling occurred in the warmer months of June and July in the north central Gulf of Mexico, likely leading to the negative relationship observed between surface temperature and larval swordfish catch. The response curve for SSHA shows the highest probability of catch around 0.17 m, the same SSHA referenced as indicating the outer Loop Current boundary (Fig. 5b). This supports the hypothesis that the Loop Current is used as

larval habitat (Leben and Born, 1993; Berger *et al.,* 1996; Hamilton *et al.,* 2000; Leben *et al.,* 2002). This is inconsistent with the findings of Rooker *et al.,* (2012) which found larval swordfish catch to be highest at negative sea surface height anomalies. However, in 2012 we observed swordfish larvae in northcentral Gulf of Mexico waters in waters with a negative sea surface height anomaly, yet near the Loop Current boundary (Fig. 6). Therefore, it is possible that the increased probability of larval swordfish catch Rooker *et al.,* (2012) observed in the northern Gulf of Mexico is specific to this smaller region and is not consistent throughout the larger spatial extent of larval swordfish habitat. Further, Rooker *et al.,* (2012) did show a negative relationship with distance from the Loop Current, suggesting that the Loop Current was important larval swordfish habitat, corroborating our findings (2012). Eddy kinetic energy (EKE) shows highest probability of catch, though minimal, near zero eddy kinetic energy (Fig. 5c). This would be the case in a water mass that exhibits very little meridional or zonal flow such as common water or fronts (Ducet and Le Traon, 2001). The fastest moving waters of boundary currents and eddies display higher EKE values, suggesting these regions may not represent larval swordfish habitat (Richardson, 2005). However, it is worth noting that the deviance explained by EKE was low (0.1%) and the significance of this parameter may have changed if we were able to incorporate more stations into model formation near the Yucatan Channel in 2010 (Table 3; Fig. 2).

An overview of our sampling and modeling indicate that swordfish do not rely heavily on mesoscale eddies for spawning and larval habitat. Instead, swordfish larvae remain near and within large current systems, a significant development in understanding larval swordfish ecology. Mesoscale eddies were sampled during our collections and are common hydrographic features in the Gulf of Mexico and Caribbean Sea (Hurlburt and Thompson, 1982; Vukovich and

Maul, 1985; Carton and Chao, 1999). These eddies are often used for spawning and larval transport of pelagic fishes, such as bluefin tuna and billfishes (Richardson *et al.,* 2009; Govoni *et al.,* 2010; Muhling *et al.,* 2010). Therefore, the use of large currents as opposed to mesoscale eddies for spawning and larval habitat by swordfish represents a life history strategy unique from other pelagic predatory fishes. These observed patterns of swordfish spawning near fast-moving currents are similar to the spawning patterns of swordfish in the Mediterranean, where swordfish spawn near areas with high current velocity such as the Straits of Messina (Megalofonou *et al.,* 1995; Relini *et al.,* 2003). This suggests that spawning near fast-moving currents is a strategy that is not unique to the North Atlantic swordfish population.

The warm temperatures of boundary currents can lead to increased growth rates for fish larvae, which is advantageous for outgrowing a larval stage with abundant predators (Bailey and Houde, 1989; Houde, 1989). However, to sustain fast growth rates in warm waters, larvae need ample prey. Boundaries associated with current systems represent convergence zones that concentrate fish larvae and zooplankton, the prey of swordfish larvae (Bakun, 2006). Thus, swordfish larvae may use the boundaries of major currents both for their warm waters and prey abundance (Fig. 6). Specifically, the Loop Current boundary contains large numbers of *Oithona* spp. copepods, a known prey item of pre-flexion swordfish larvae (Govoni *et al.,* 2003; Rathmell, 2007). The presence of neustonic flyingfish (Exocoetidae) and subsurface tuna and mackerel (Scombridae) larvae may make these boundaries ideal habitat for swordfish larvae as they transition to piscivory (Arata, 1954; Gorbunova, 1969; Richards *et al.,* 1993; Govoni *et al.,* 2003). However, convergence zones often lead to increased predation pressure and may increase mortality of swordfish larvae, representing a trade-off between increased food availability and predation (Bakun, 2006).

Further, small larvae (< 6 mm SL) were primarily caught north of Honduras, in the Yucatan Channel, and the northern and western extents of the Loop Current, with larger larvae (> 6 mm SL) occurring on the eastern side of the Loop Current (Fig. 4). However, there was a great degree of variability in this trend, suggesting that there are multiple spawning locations throughout the region including the near the Caribbean Current, Yucatan Channel, and the Gulf of Mexico, corroborating suggestions of these spawning locations from previous studies (Arocha, 1997; Govoni et al., 2003; Arocha, 2007). The general trend of presence of swordfish larvae in the fast-moving boundary currents and larger larvae occurring in the eastern extent of the Loop Current supports the assertion that these boundary currents provide a means to transport larvae further along the western boundary current system of the Atlantic. Data from the NOAA Pelagic Observer Program indicate that the northern Gulf of Mexico and coastal Atlantic waters of the southeastern United States are predominately occupied by juvenile swordfish (80-130 cm; Muhling *et al.,* 2015). Multiple studies have also indicated that the northern Gulf of Mexico and the waters off the southeastern United States, particularly the Charleston Bump, represent juvenile habitat (Cramer, 2001; Govoni *et al.,* 2003). These boundary currents can thus serve a dual purpose as habitat for swordfish larvae and a mechanism to transport larvae toward their juvenile habitat.

Transport of swordfish larvae to juvenile habitat from spawning in or near fast-moving boundary currents well fits the member vagrant hypothesis as larvae spawned in varying locations throughout the Caribbean, Gulf of Mexico, and Straits of Florida will likely be transported to similar locations to begin the later stages of development (Sinclair, 1988). However, swordfish in the North Atlantic are still genetically identified as one population, thus the boundary currents alone do not represent a complete closure of this population because North

Atlantic swordfish also spawn south of the Sargasso Sea which likely transports larvae to additional juvenile habitat in the southeastern Caribbean (Arocha, 1997; Bremer *et al.,* 2005; Arocha, 2007). Swordfish which spawn near these boundary currents and those that spawn in the Sargasso Sea are considered different spawning groups and mixing among the two spawning groups may not occur until the fish move farther north to adult foraging grounds (Arocha, 2007).

Furthermore, adult swordfish need to be able to detect these boundary currents while they are at their day-time depths (up to 900 m) to ensure they remain in proximity to preferred spawning locations. These fish may be able to remain near the western boundary current system through sensing temperature gradients both near the surface and at depth (Podesta *et al.,* 1993; Sheinbaum *et al.,* 2002; Carrillo *et al.,* 2016). Therefore, large current regimes, such as the Yucatan Current, may represent as spatially stable and easily identifiable region for swordfish to spawn. Fecund swordfish and swordfish eggs are often caught near these boundary currents, particularly those of the Yucatan Current, furthering evidence that these boundaries represent spawning habitat (Arocha, 1997; 2007; Leyva-Cruz *et al.,* 2016). Small swordfish larvae were caught within the boundary currents in multiple regions and the size of swordfish larvae also tends to increase as they are further downstream in the boundary current systems, supporting the assertion that these boundary currents are important oceanographic features for swordfish spawning. While presence of larvae in these boundaries does not directly translate to adult swordfish presence, the presence of swordfish eggs and catches of fecund adult swordfish suggest these current boundaries are important for both swordfish spawning and larval habitat.

The relationship between catchability of swordfish larvae and fraction of lunar illumination suggest a connection between the lunar phase and time of spawning of swordfish. Highest catchability of small (65% of larvae <6 mm SL) swordfish larvae occurred during

crescent and gibbous moon phases. The high catches of larvae during crescent and gibbous moons could be a result of spawning during the quarter moon phases given an estimate of three days prior to hatching and the subsequent growth rate of swordfish larvae (Yasuda *et al*., 1978; Enfield and Mayer, 1997; Govoni *et al.,* 2003). Multiple reports show catch per unit effort (CPUE) increases for the swordfish fishery around first and third quarter moon phases, possibly indicative of spawning as CPUE is often highest for fisheries during spawning (dos Santos and Garcia, 2005; Yukami *et al.,* 2009; Poisson *et al.,* 2010; Erisman *et al.,* 2011). The strong correlation of night time depth of adult swordfish with lunar illumination supports the hypothesis that the lunar cycle influences the behavior of swordfish (Dewar *et al.*, 2011; Lerner *et al*., 2013). While the exact spawning time of swordfish is uncertain, our data reveal the importance of lunar illumination for the spawning of swordfish for the first time.

The peak in larval swordfish catch at noon was consistent with observations from Habtes *et al.* (2014; Fig. 5e). Diel variability in catch of ichthyoplankton in surface water is often due to diel vertical migration of ichthyoplankton. However, the diet of swordfish larvae suggests a shallow water existence as young larvae consume neritic copepods and larger larvae are piscivorous, suggesting a neustonic lifestyle (Arata, 1954; Gorbunova, 1969; Govoni *et al.,* 2003). Thus, while it is difficult to elucidate a reason for the diel trend in larval swordfish catch, the literature suggests that large scale vertical migrations are unlikely and our results may be an artifact of sampling otherwise favorable habitat at these hours.

Mapping and habitat models from this study corroborate previous work indicating that there are oceanographic features throughout the Gulf of Mexico and western Caribbean Sea that serve as favorable habitat for swordfish larvae. Future work to better understand the habitat associations of swordfish larvae should focus on sampling multiple oceanographic features to

attain better knowledge of their larval distribution throughout the Caribbean Current, Yucatan Current, and Loop Current. Obtaining finer resolution data on the exact water masses and fronts utilized by these fish for spawning and larval habitat can be used to protect regions from fishing pressure and shipping disturbance to assist the reproductive success of these fish. However, intra-annual variability of swordfish spawning needs to be assessed, thus sampling should occur January through July with a focus on both eggs and larvae in order to elucidate this variation (Govoni *et al.,* 2003; Rooker *et al.,* 2012; Neilson *et al*., 2014). Habitat models may also be constructed through different methodologies to incorporate historical data from SEAMAP and Marine Resources Monitoring, Assessment, and Prediction program (MARMAP) data sets but these must be done carefully to ensure the physical parameters are accurate and precise. The years of sampling in this study (2010-2012) also occurred at a time of low abundance in the North Atlantic swordfish stock, though recovery of the stock was likely occurring (ICCAT, 2014). Future studies should assess how and if habitat models of larvae may change as the stock size fluctuates and if the quantity of favorable habitat as predicted by these models relates to recruitment of this stock.

We present new developments in the understanding of the early life history of swordfish. This study supports and expands the spatial extent of the existing hypothesis that larval swordfish habitat is associated with boundary currents in the western Caribbean Sea and Gulf of Mexico, primarily the Caribbean, Yucatan, and Loop Currents and that these currents may provide a means to transport swordfish larvae toward larval and juvenile habitats. Assessment of the standard length of larvae caught throughout the sampling region indicated that multiple spawning locations likely occur, with small larvae caught north of Honduras, the Yucatan Channel, and in the north central Gulf of Mexico in northern and western extents of the Loop

current. We also indicate a connection between lunar illumination and swordfish spawning, the first assertion of such a connection to our knowledge. While higher resolution data should be used to further identify smaller scale associations of swordfish larvae with oceanographic features, the identification of larval habitat from this study is a step toward an improved understanding of this commercially and ecologically important species. This study provides valuable information about the larval habitat of a commercially important species so that estimations of anthropogenic influences on larval habitat can be made, including severely deleterious events such as oil spills.

ACKNOWLEDGMENTS:

The authors would like to thank the lab at the NOAA Fisheries Oceanography for Recruitment, Climate and Ecosystem Studies (FORCES), the taxonomists at the Departamento de Sistemática y Ecología Acuática at El Colegio de la Frontera Sur (ECOSUR), the staff at the Polish Plankton Sorting and Identification Center in Szczecin, Poland, and the officers and crew of the NOAA ship Gordon Gunter that facilitated data collection on the SEAMAP cruises. The authors would also like to thank J Serafy for useful comments to improve this manuscript. This research was carried out under the auspices of the Cooperative Institute for Marine and Atmospheric Studies, University of Miami and partially funded by NASA (NNX11AP76G, NNX08AL06G), and the NOAA Southeast Fisheries Science Center. No authors have any conflicts of interest to declare.

REFERENCES:

Arata Jr, G. F. (1954). A contribution to the life history of the swordfish, *Xiphias gladius* Linnaeus, from the South Atlantic coast of the United States and the Gulf of Mexico. *Bulletin of Maine Science 4,* 183-243.

Arocha, F. (1997). The reproductive dynamics of swordfish *Xiphias gladius* L and management implications in the northwestern Atlantic. PhD thesis, University of Miami

Arocha, F. (2007). Swordfish reproduction in the Atlantic Ocean: an overview. *Gulf and Caribbean Research*, *19*, 21-36.

Bakun, A. (1996). *Patterns in the ocean*. La Paz, Mexico: California Sea Grant, in cooperation with Centro de Investigaciones Biologicas del Noroeste

Bakun, A. (2006). Fronts and eddies as key structures in the habitat of marine fish larvae: opportunity, adaptive response and competitive advantage. *Scientia Marina*, *70*, 105-122.

Bailey, K. M., & Houde, E. D. (1989). Predation on eggs and larvae of marine fishes and the recruitment problem. *Advances in Marine Biology*, *25*, 1-83.

Barry, S. C., & Welsh, A. H. (2002). Generalized additive modelling and zero inflated count data. *Ecological Modelling 157*, 179-188.

Berger, T. J., P. Hamilton, J. J. Singer, R. R. Leben, G. H. Born & C. A. Fox (1996), Louisiana/Texas Shelf Physical Oceanography Program Eddy Circulation Study: Final Synthesis Report. Volume I: Technical Report, OCS Study MMS 96-0051, U.S. Dept. of the Interior, Minerals Management Service, Gulf of Mexico OCS Region, New Orleans, LA. 324 pp.

Bremer, J. A., Mejuto, J., Gómez-Márquez, J., Boán, F., Carpintero, P., Rodríguez, J. M., Viñas, J., Greig, T.W., & Ely, B. (2005). Hierarchical analyses of genetic variation of samples from breeding and feeding grounds confirm the genetic partitioning of northwest Atlantic and South Atlantic populations of swordfish (*Xiphias gladius* L.). *Journal of Experimental Marine Biology and Ecology*, *327*, 167-182.

Burnham, K. P., & Anderson, D. R. (2002). Akaike Weights. In *Model Selection and Multimodel Inference*: *A Practical Information-Theoretic Approach Second Edition* (pp. 60-65). Springer: New York.

Candela, J., Sheinbaum, J., Ochoa, J., Badan, A., & Leben, R. (2002). The potential vorticity flux through the Yucatan Channel and the Loop Current in the Gulf of Mexico. *Geophysical Research Letters*, *29*(22).

Carrillo, L., Johns, E. M., Smith, R. H., Lamkin, J. T., & Largier, J. L. (2016). Pathways and hydrography in the Mesoamerican Barrier Reef System Part 2: Water masses and thermohaline structure. *Continental Shelf Research, 120*, 41-58.

Carton, J. A., & Chao, Y. (1999). Caribbean Sea eddies inferred from TOPEX/Poseidon altimetry and a 1/6 Atlantic Ocean model simulation. *Journal of Geophysical Research*, *104*(C4), 7743-7752.

Chancollon, O., Pusineri, C., & Ridoux, V. (2006). Food and feeding ecology of Northeast Atlantic swordfish (*Xiphias gladius*) off the Bay of Biscay. *ICES Journal of Marine Science: Journal du Conseil. 63*, 1075-1085.

Chassignet, E. P., Hurlburt, H. E., Smedstad, O. M., Halliwell, G. R., Hogan, P. J., Wallcraft, A. J., Baraille, R., & Bleck, R. (2007). The HYCOM (hybrid coordinate ocean model) data assimilative system. *Journal of Marine Systems, 65*, 60-83.

Cramer, J. (2001). Geographic distribution of longline effort and swordfish discard rates in the straits of Florida and oceanic waters of the continental shelf, slope, and Blake Plateau off Georgia and the Carolinas from 1991 to 1995. In *American Fisheries Society Symposium*, 97-104

Cushing, D. H. (1969). The regularity of the spawning season of some fishes. *ICES Journal of Marine Science: Journal du Conseil, 33*, 81-92.

Cushing, D. H. (1990). Plankton production and year-class strength in fish populations: an update of the match/mismatch hypothesis. *Advances in Marine Biology, 26,* 249-293.

Dewar, H., Prince, E. D., Musyl, M. K., Brill, R. W., Sepulveda, C., Luo, J., Foley,D., Orbesen, E.S., Dromeier, M.L.,Nasby-Lucas, N., Snodgrass, D., Luars, R.M., Hoolihan, J.P. Block, B.A., & McNaughton, L.M. (2011). Movements and behaviors of swordfish in the Atlantic and Pacific Oceans examined using pop□up satellite archival tags. *Fisheries Oceanography 20*, 219-241.

Domingues, R., Goni, G., Bringas, F., Muhling, B., Lindo□Atichati, D., & Walter, J. (2016). Variability of preferred environmental conditions for Atlantic bluefin tuna (Thunnus thynnus) larvae in the Gulf of Mexico during 1993–2011. *Fisheries Oceanography*, *25*, 320-336.

Ducet, N., & Le Traon, P. Y. (2001). A comparison of surface eddy kinetic energy and Reynolds stresses in the Gulf Stream and the Kuroshio Current systems from merged TOPEX/Poseidon and ERS-1/2 altimetric data. *Journal of Geophysical Research-Oceans*, *106,* 16603-16622.

Enfield, D. B., & Mayer, D. A. (1997). Tropical Atlantic sea surface temperature variability and its relation to El Niño□Southern Oscillation. *Journal of Geophysical Research-Oceans 102*, 929-945.

Erisman, B. E., Allen, L. G., Claisse, J. T., Pondella, D. J., Miller, E. F., & Murray, J. H. (2011). The illusion of plenty: hyperstability masks collapses in two recreational fisheries that target fish spawning aggregations. *Canadian Journal of Fisheries and Aquatic Sciences*, *68*, 1705-1716.

Feng, J., Durant, J. M., Stige, L. C., Hessen, D. O., Hjermann, D. Ø., Zhu, L., Llope, M., & Stenseth, N.C. (2015). Contrasting correlation patterns between environmental factors and chlorophyll levels in the global ocean. *Global Biogeochemical Cycles 29*, 2095-2107

Garcia, H. E., & Gordon, L. I. (1992). Oxygen solubility in seawater: Better fitting equations. *Limnology and Oceanography, 37,* 1307-1312.

Gorbunova, N. N. (1969). Breeding grounds and food of the larvae of the swordfish [*Xiphias gladius* Linné (Pisces, Xiphilidae)]. *Problems in Ichthyology*, *9*, 375-387.

Govoni, J. J., Stender, B. W., & Pashuk, O. (2000). Distribution of larval swordfish, *Xiphias gladius*, and probable spawning off the southeastern United States. *Fishery Bulletin, 98*, 64-74

Govoni, J. J., Laban, E. H., & Hare, J. A. (2003). The early life history of swordfish (*Xiphias gladius*) in the western North Atlantic. *Fishery Bulletin, 101*, 778-789.

Govoni, J. J., Hare, J. A., Davenport, E. D., Chen, M. H., & Marancik, K. E. (2010). Mesoscale, cyclonic eddies as larval fish habitat along the southeast United States shelf: a Lagrangian description of the zooplankton community. *ICES Journal of Marine Science: Journal du Conseil. 67*, 403-411.

Grall, C., De Sylva, D. P., & Houde, E. D. (1983). Distribution, relative abundance, and seasonality of swordfish larvae. *Transactions of American Fisheries Society*, *112*, 235-246.

Habtes, S., Muller□Karger, F. E., Roffer, M. A., Lamkin, J. T., & Muhling, B. A. (2014). A comparison of sampling methods for larvae of medium and large epipelagic fish species during spring SEAMAP ichthyoplankton surveys in the Gulf of Mexico. *Limnology and Oceanography: Methods*, *12*, 86-101.

Hamilton, P., Berger, T.J., Singer, J.J., Waddell, E., Churchill, J.H., Leben, R.R., Lee, T.N., & Sturges, W., (2000). DeSoto Canyon Eddy Intrusion Study, Final Report, Volume II: Technical Report, OSC Study MMS 2000-080. US Department of the Interior, Minerals Management Service, Gulf of Mexico OCS Region, New Orleans, LA, 275pp.

Hernandez Jr, F. J., Powers, S. P., & Graham, W. M. (2010). Seasonal variability in ichthyoplankton abundance and assemblage composition in the northern Gulf of Mexico off Alabama. *Fishery Bulletin*, *108*(2), 193-207.

Houde, E. D., Dowd, J. C., Berkeley, C. E., Houde, S. A. E. D., & James, C.(1979). *Ichthyoplankton abundance and diversity in the eastern Gulf of Mexico* (No. 574.92 I2).

Houde, E. D. (1989). Comparative growth, mortality, and energetics of marine fish larvae: temperature and implied latitudinal effects. *Fishery Bulletin*, *87*, 471-495.

Huberty, C. J. (1994). *Applied discriminant analysis* (Vol. 297). Wiley-Interscience.

Hurlburt, H. E., & Thompson, J.D. (1982). The dynamics of the loop current and shed eddies in a numerical model of the Gulf of Mexico. In: *Hydrodynamics of Semi-enclosed Seas, ed. J. C. J. Nihoul, Elsevier Science*, New York, NY., 243–297

International Commission for the Conservation of Atlantic Tunas (2014). Report of the ICCAT swordfish stock assessment session.

Ito, R. Y., Dollar, R. A., & Kawamoto, K. E. (1998). The Hawaii-based longline fishery for swordfish, *Xiphias gladius*. *Biology and fisheries of swordfish, Xiphias gladius. NOAA Tech Rep NMFS*, *142*, 77-88.

Leben, R. R., & Born, G. H. (1993). Tracking Loop Current eddies with satellite altimetry. *Advances in Space Research*, *13*, 325-333.

Leben, R. R., Born, G. H., & Engebreth, B. R. (2002). Operational altimeter data processing for mesoscale monitoring. *Marine Geodesy*, *25*, 3-18.

Lerner, J. D., Kerstetter, D. W., Prince, E. D., Talaue-McManus, L., Orbesen, E. S., Mariano, A., Snodgrass, D., & Thomas, G. L. (2013). Swordfish vertical distribution and habitat use in relation to diel and lunar cycles in the western North Atlantic. *Transactions of the American Fisheries Society*, *142*, 95-104.

Leyva-Cruz, E., Vásquez-Yeomans, L., Carrillo, L., & Valdez-Moreno, M. (2016). Identifying pelagic fish eggs in the southeast Yucatan Peninsula using DNA barcodes. *Genome*, *59*, 1117-1129.

Megalofonou, P., Dean, J. M., De Metrio, G., Wilson, C., & Berkeley, S. (1995). Age and growth of juvenile swordfish, *Xiphias gladius* Linnaeus, from the Mediterranean Sea. *Journal of Experimental Marine Biology and Ecology*, *188*(1), 79-88.

Muhling, B. A., Lamkin, J. T., & Roffer, M. A. (2010). Predicting the occurrence of Atlantic bluefin tuna (*Thunnus thynnus*) larvae in the northern Gulf of Mexico: building a classification model from archival data. *Fisheries Oceanography*, *19*, 526-539.

Muhling, B. A., Lamkin, J. T., & Richards, W. J. (2012). Decadal-scale responses of larval fish assemblages to multiple ecosystem processes in the northern Gulf of Mexico. *Marine Ecology Progress Series*, *450*, 37-53.

Muhling, B. A., Liu, Y., Lee, S. K., Lamkin, J. T., Malca, E., Llopiz, J.K., Ingram G. W., Quattro J. M., Walter, J. F., Doering, K., Roffer, M. A., & Muller-Karger, F. (2015). Past, Ongoing and Future Research on Climate Change Impacts on Tuna and Billfishes in the Western Atlantic. *Collect. Vol. Sci. Pap. ICCAT*, *71*, 147-174.

Nakamura, I. (1985) Billfishes of the world. FAO Fish. Synop. *125*, 58 p

NASA Goddard Space Flight Center, Ocean Ecology Laboratory, Ocean Biology Processing Group. Moderate-resolution Imaging Spectroradiometer (MODIS) Aqua Chlorophyll Data; 2014 Reprocessing. NASA OB.DAAC, Greenbelt, MD, USA. doi: 10.5067/AQUA/MODIS/L3M/CHL/2014. Accessed on 03/2016

Neilson, J. D., Loefer, J., Prince, E. D., Royer, F., Calmettes, B., Gaspar, P., Lopez, R., & Andrushchenko, I. (2014). Seasonal Distributions and Migrations of Northwest Atlantic Swordfish: Inferences from Integration of Pop-Up Satellite Archival Tagging Studies. *PloS one*, *9*, e112736.

Oey, L. Y., Ezer, T., & Lee, H. C. (2005). Loop Current, rings and related circulation in the Gulf of Mexico: A review of numerical models and future challenges. *Circulation in the Gulf of Mexico: Observations and models*, Washington D.C: AGU

Palko, R. J., G. L. Beardsley, & W. J. Richards. (1981) Synopsis of the biology of the swordfish *Xiphias gladius* Linnaeus. U.S. Dep. Commer. NOAATech. Rep. NMFS Circ. 441.

Podestá, G. P., Browder, J. A., & Hoey, J. J. (1993). Exploring the association between swordfish catch rates and thermal fronts on US longline grounds in the western North Atlantic. *Continental Shelf Research 13*, 253-277.

Poisson, F., Gaertner, J. C., Taquet, M., Durbec, J. P., and Bigelow, K. (2010). Effects of lunar cycle and fishing operations on longline-caught pelagic fish: fishing performance, capture time, and survival of fish. *Fishery Bulletin 108*, 268-281.

Rathmell, K. (2007). The influence of the Loop Current on the diversity, abundance, and distribution of zooplankton in the Gulf of Mexico. Master's thesis, University of South Florida.

Relini, L. O., Palandri, G., & Garibaldi, F. (2003). Reproductive parameters of the Mediterranean swordfish. *Bioiogia . Marina Mediterranea, 10*(2), 210-222.

Richards, W. J., McGowan, M. F., Leming, T., Lamkin, J. T., & Kelley, S. (1993). Larval fish assemblages at the Loop Current boundary in the Gulf of Mexico. *Bulletin of Marine Science*, *53*, 475-537.

Richardson, P. L. (2005). Caribbean Current and eddies as observed by surface drifters. *Deep-Sea Research Pt. II*, *52*, 429-463.

Richardson, D. E., Llopiz, J. K., Leaman, K. D., Vertes, P. S., Muller-Karger, F. E., & Cowen, R. K. (2009). Sailfish (*Istiophorus platypterus*) spawning and larval environment in a Florida Current frontal eddy. *Progress in Oceanography, 82*, 252-264.

Richardson, D. E., Llopiz, J. K., Guigand, C. M., & Cowen, R. K. (2010). Larval assemblages of large and medium-sized pelagic species in the Straits of Florida. *Progress in Oceanography, 86*, 8-20.

Roberts, J. J., Best, B. D., Dunn, D. C., Treml, E. A., & Halpin, P. N. (2010). Marine Geospatial Ecology Tools: An integrated framework for ecological geoprocessing with ArcGIS, Python, R, MATLAB, and C++. *Environmental Modelling & Software*, *25*, 1197-1207.

Rooker, J. R., Simms, J. R., Wells, R. D., Holt, S. A., Holt, G. J., Graves, J. E., & Furey, N. B. (2012). Distribution and habitat associations of billfish and swordfish larvae across mesoscale features in the Gulf of Mexico. *PloS one*, *7*, e34180.

dos Santos, M. N., & Garcia, A. (2005). The influence of the moon phase on the CPUEs for the Portuguese swordfish (*Xiphias gladius* L., 1758) fishery. *Col. Vol. Sci. Pap. ICCAT*, *58*, 1466-1469.

Scott, W. B., & Tibbo, S. N. (1968). Food and feeding habits of swordfish, *Xiphias gladius*, in the western North Atlantic. *Journal of the Fisheries Board of Canada*, *25,* 903-919.

Sheinbaum, J., Candela, J., Badan, A., & Ochoa, J. (2002). Flow structure and transport in the Yucatan Channel. *Geophysical Research Letters 29,* 101-104

Simms, J. R., Rooker, J. R., Holt, S. A., Holt, G. J., & Bangma, J. (2010). Distribution, growth, and mortality of sailfish (*Istiophorus platypterus*) larvae in the northern Gulf of Mexico. *Fishery Bulletin, 108*, 478-490.

Sinclair, M. (1988). *Marine populations: an essay on population regulation and speciation*. Washington Press.

Solanki, H. U., Bhatpuria, D., & Chauhan, P. (2015). Integrative Analysis of AltiKa-SSHa, MODIS-SST, and OCM-Chlorophyll Signatures for Fisheries Applications. *Marine Geodesy*, *38,* 672-683.

Sundblad, G., Härmä, M., Lappalainen, A., Urho, L., & Bergström, U. (2009). Transferability of predictive fish distribution models in two coastal systems. *Estuarine, Coastal and Shelf Science*, *83*, 90-96.

Taylor, R. G., & Murphy, M. D. (1992). Reproductive biology of the swordfish *Xiphias gladius* in the Straits of Florida and adjacent waters. *Fishery Bulletin, 90,* 809-816.

Teo, S. L., Boustany, A. M., & Block, B. A. (2007). Oceanographic preferences of Atlantic bluefin tuna, *Thunnus thynnus*, on their Gulf of Mexico breeding grounds. *Marine Geodesy, 152,* 1105-1119.

Vukovich, F. M., & Maul, G. A. (1985). Cyclonic eddies in the eastern Gulf of Mexico. *Journal of Physical Oceanography, 15,* 105-117.

Ward, P., Porter, J. M., & Elscot, S. (2000). Broadbill swordfish: status of established fisheries and lessons for developing fisheries. *Fish and Fisheries, 1*, 317-336.

Wood, S. N. (2008). Fast stable direct fitting and smoothness selection for generalized additive models. *Journal of the Royal Statistical Society Series B Statistical Methodology 70*, 495-518.

Wood, S.N. (2017). *Generalized additive models: an introduction with R*. CRC press.

Yasuda F, Kohno H, Yatsu A, Ida H, Arena P, Li Greci F, Taki Y (1978) Embryonic and early larval stages of the swordfish, *Xiphias gladius*, from the Mediterranean. *Journal of the Tokyo University of Fisheries*, *65*, 91–97

Yukami, R., Ohshimo, S., Yoda, M., & Hiyama, Y. (2009). Estimation of the spawning grounds of chub mackerel *Scomber japonicus* and spotted mackerel *Scomber australasicus* in the East China Sea based on catch statistics and biometric data. *Fisheries Science*, *75*, 167-174.

Zuur, A. F., Ieno, E. N., Walker, N. J., Saveliev, A. A., & Smith, G. M. (2009). Zero-truncated and zero-inflated models for count data. In *Mixed effects models and extensions in ecology with R* (pp. 261-293). New York: Springer

Zuur, A.F. (2012) *A beginner's guide to generalized additive models with R*. Newburgh: Highland Statistics Limited.

TABLES:

Table 1: Environmental parameters used in model formation with sources and metrics listed. All *in-situ* data were collected using a Seabird SBE 9/11 Plus CTD (conductivity, temperature, and depth) equipped with a dissolved oxygen sensor (SBE 43).

Parameter	Source	Minimum	Maximum	Mean	Median
Eddy Kinetic Energy ($m^2 s^{-2}$)	HYCOM	0.00	1.54	0.14	0.06
Sea Surface Height Anomaly (m)	HYCOM	-0.45	0.64	-0.09	-0.19
Temperature at 5 m (^oC)	*In-situ*	21.45	28.35	26.39	26.66
Salinity at 5 m	*In-situ*	33.04	36.70	36.04	36.02
Oxygen at 5 m (mg L^{-1})	*In-situ*	6.13	7.46	6.60	6.61
Chlorophyll *a* (mg m^{-3})	MODIS	0.04	0.57	0.11	0.10
Depth (m)	NCEI	204.00	7124.00	2177.24	2140.50

Table 2: Details of the backward stepwise Akaike Information Criterion (ΔAIC) model selection process including the original model and the subsequent top three models for each iteration as determined by greatest change in AIC and deviance explained. The overall best fit model for the final iteration is in bold. ORT represents oxygen residuals from temperature. CRT (RE) represents chlorophyll *a* residuals from temperature as a random effect.

Iteration	Variables Included	AIC (Δ)	DE (Δ)	Akaike Weight(w_i)
1	Temperature, ORT, CRT (RE), SSHA, EKE, Lun Illum, Salinity, Hour, Depth, Year, Long/Lat(TE)	296.33 (0)	33.6(0)	0.126
1	Temperature, ORT, CRT (RE), SSHA, EKE, Lun Illum, Salinity, Hour, Depth, Long/Lat(TE)	295.04(-1.29)	33.1(-0.5)	0.228
1	Temperature, CRT (RE), SSHA, EKE, Lun Illum, Salinity, Hour, Depth, Year, Long/Lat(TE)	294.61(-1.72)	33.2(-0.3)	0.282
1	Temperature, ORT, CRT (RE), SSHA, EKE, Lun Illum, Hour, Depth, Year, Long/Lat(TE)	294.53(-1.80)	33.5(-0.1)	0.294
2	Temperature, ORT, CRT (RE), SSHA, EKE, Lun Illum, Hour, Depth Year, Long/Lat(TE)	294.53(-1.80)	33.5(-0.1)	0.173
2	Temperature, ORT, CRT (RE), SSHA, EKE, Lun Illum, Salinity, Hour, Year, Long/Lat(TE)	296.54(0.210)	30.5(-3.1)	0.063
2	Temperature, ORT, CRT (RE), SSHA, EKE, Lun Illum, Hour, Depth, Long/Lat(TE)	293.43(-2.89)	33(-0.6)	0.299
2	Temperature, CRT (RE), SSHA, EKE, Lun Illum, Hour, Depth, Year, Long/Lat(TE)	292.74(-3.58)	33.2(-0.3)	0.423
3	Temperature, CRT (RE), SSHA, EKE, Lun Illum, Hour, Depth, Year, Long/Lat(TE)	292.74(-3.58)	33.2(-0.3)	0.217
3	Temperature, CRT (RE), SSHA, Lun Illum, Hour, Depth, Year, Long/Lat(TE)	296.66(0.330)	29.4(-4.2)	0.008
3	Temperature, CRT (RE) SSHA, EKE, Lun Illum, Salinity, Hour, Depth, Long/Lat(TE)	292.1(-4.22)	33.1(-0.5)	0.298
3	Temperature, CRT (RE), SSHA, EKE, Lun Illum, Hour, Year, Long/Lat(TE)	291.31(-5.01)	33.1(-0.5)	0.443
4	Temperature, CRT (RE), SSHA, EKE, Lun Illum,, Hour, Year, Long/Lat(TE)	291.31(-5.01)	33.1(-0.5)	0.380
4	Temperature, CRT (RE), EKE, Lun Illum, Hour, Year, Long/Lat(TE)	298(1.670)	30(-3.6)	0.013
4	Temperature, CRT (RE), SSHA, Lun Illum, Hour, Year, Long/Lat(TE)	295.93(-0.39)	29.4(-4.2)	0.038
4	Temperature, CRT (RE), SSHA, EKE, Lun Illum, Hour, Long/Lat(TE)	290.54(-5.78)	33.1(-0.5)	0.558
5	**Temperature, CRT (RE), SSHA, EKE, Lun Illum, Hour, Long/Lat(TE)**	**290.54(-5.78)**	**33.1(-0.5)**	**0.780**
5	Temperature, SSHA, EKE, Lun Illum, Hour, Long/Lat(TE)	298.64(2.31)	30.6(-3)	0.010
5	Temperature, CRT (RE), EKE, Lun Illum, Hour, Long/Lat(TE)	299.3(2.970)	29.2(-4.4)	0.014
5	Temperature, CRT (RE), SSHA, Lun Illum, Hour, Long/Lat(TE)	293.52(-2.81)	33.6(0)	0.176

Table 3: Change in Akaike Information Criterion (ΔAIC) and deviance explained (ΔDE) for environmental and spatial parameters in the final model.

Final Model	Variable	Δ AIC	ΔDE
AIC: 290.542	Hour of Sampling	19.02	6.3%
DE: 33.1%	Fraction of Lunar Illumination	17.91	7.7%
	Latitude, Longitude	13.65	9.7%
	Temperature at 5 m (^{o}C)	9.58	2.0%
	Sea Surface Height Anomaly (m)	8.10	1.9%
	Eddy Kinetic Energy (m^2 s^{-2})	2.98	0.1%

FIGURE LEGENDS:

Figure 1: Schematic map of the Gulf of Mexico and Caribbean Sea showing the major ocean currents. Colors depict mean sea surface temperature estimates from the Hybrid Ocean Coordinate Model (HYCOM) 1/12^{o} Reanalysis from April and May of 2010.

Figure 2: Distribution of sampling locations in the Gulf of Mexico and Caribbean in April-May a)2010 b)2011 and c)2012. Red symbols (+) indicate stations sampled and were used as model input. Black symbols (+) indicate stations sampled and were not used as model input due to sensor malfunctions and their shallow bathymetry (< 200 m depth). Red circles ● indicate stations that showed presence of swordfish larvae and were used as model input. Black circles ● indicate stations that showed presence of swordfish larvae and were not used as model input due to sensor malfunctions, lack of CTD casts, or their shallow bathymetry (< 200 m depth). Color scale indicative of sea surface temperature (SST).

Figure 3: Correlations between A) chlorophyll- *a* and temperature at 5 m ($r=-0.49$, $p<0.01$ and B) dissolved oxygen at 5 m and temperature at 5 m ($r=-0.74$, $p<0.01$).

Figure 4: Mean standard length of swordfish larvae by station caught in both neuston and S-10 nets from 2010-2012. Color scale indicative of sea surface temperature (SST).

Figure 5: The response curves for a) temperature at 5m (^{o}C), b) sea surface height anomaly (m), c) eddy kinetic energy ($m^2\ s^{-2}$), d) fraction of lunar illumination with the dark circle indicating the new moon and the open circle representing the full moon, and e) hour of sampling, with the open circle indicating local noon.

Figure 6: Catch of swordfish larvae in the Loop Current in 2012 overlaid on sea surface height anomaly (m). Red circles (●) indicate stations that showed presence of swordfish larvae.

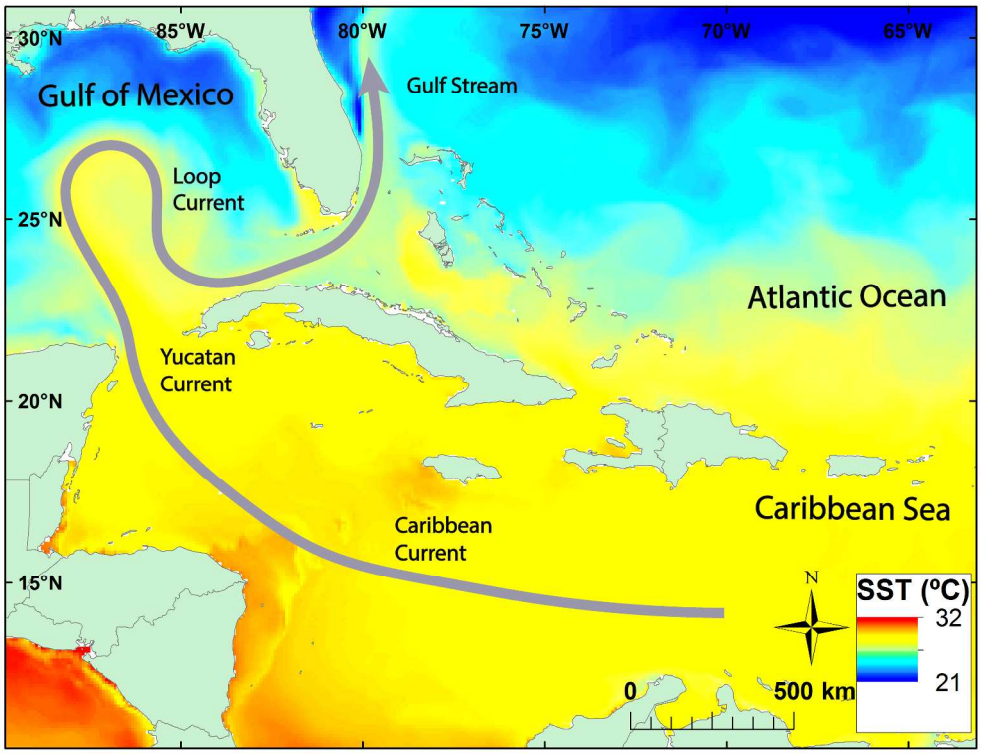

Figure 1: Schematic map of the Gulf of Mexico and Caribbean Sea showing the major ocean currents. Colors depict mean sea surface temperature estimates from the Hybrid Ocean Coordinate Model (HYCOM) 1/12o Reanalysis from April and May of 2010.

279x215mm (300 x 300 DPI)

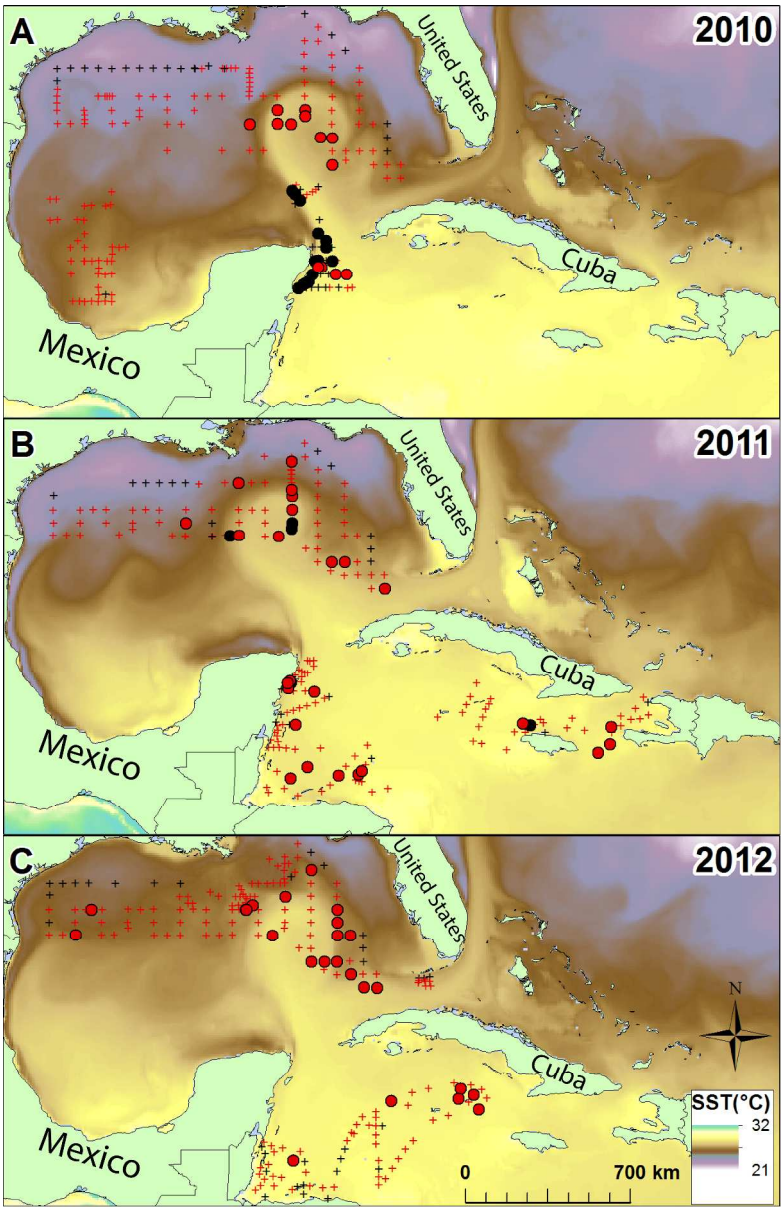

Figure 2: Distribution of sampling locations in the Gulf of Mexico and Caribbean in April-May a)2010 b)2011 and c)2012. Red symbols (+) indicate stations sampled and were used as model input. Black symbols (+) indicate stations sampled and were not used as model input due to sensor malfunctions and their shallow bathymetry (< 200 m depth). Red circles • indicate stations that showed presence of swordfish larvae and were used as model input. Black circles • indicate stations that showed presence of swordfish larvae and were not used as model input due to sensor malfunctions, lack of CTD casts, or their shallow bathymetry (< 200 m depth). Color scale indicative of sea surface temperature (SST).

279x431mm (300 x 300 DPI)

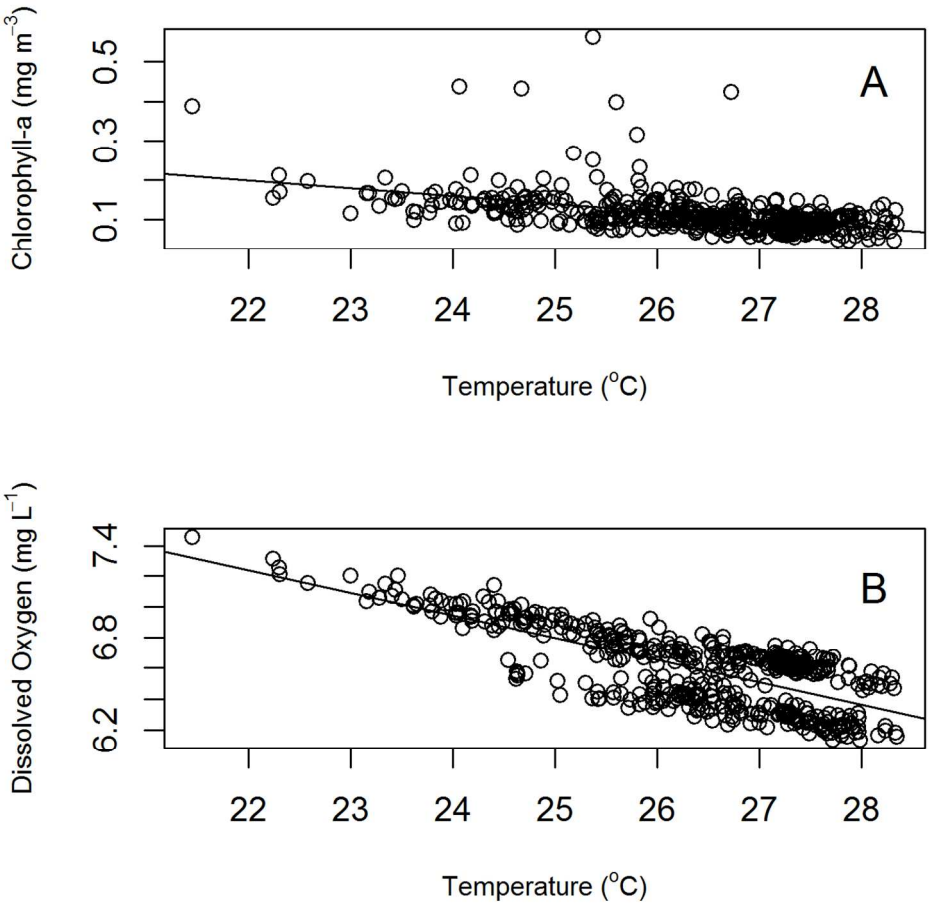

Figure 3: Correlations between A) chlorophyll- a and temperature at 5 m (r=-0.49, p<0.01 and B) dissolved oxygen at 5 m and temperature at 5 m (r=-0.74, p<0.01).

127x127mm (300 x 300 DPI)

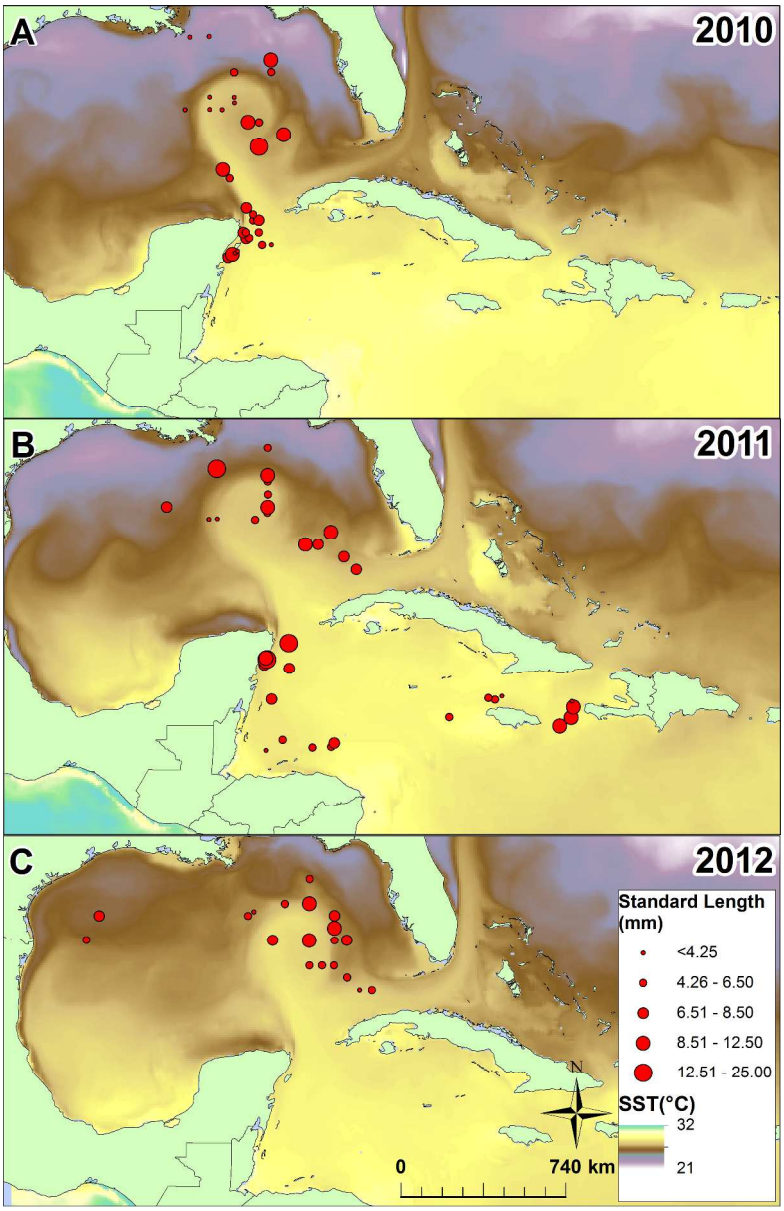

Figure 4: Mean standard length of swordfish larvae by station caught in both neuston and S-10 nets from 2010-2012. Color scale indicative of sea surface temperature (SST).

279x431mm (300 x 300 DPI)

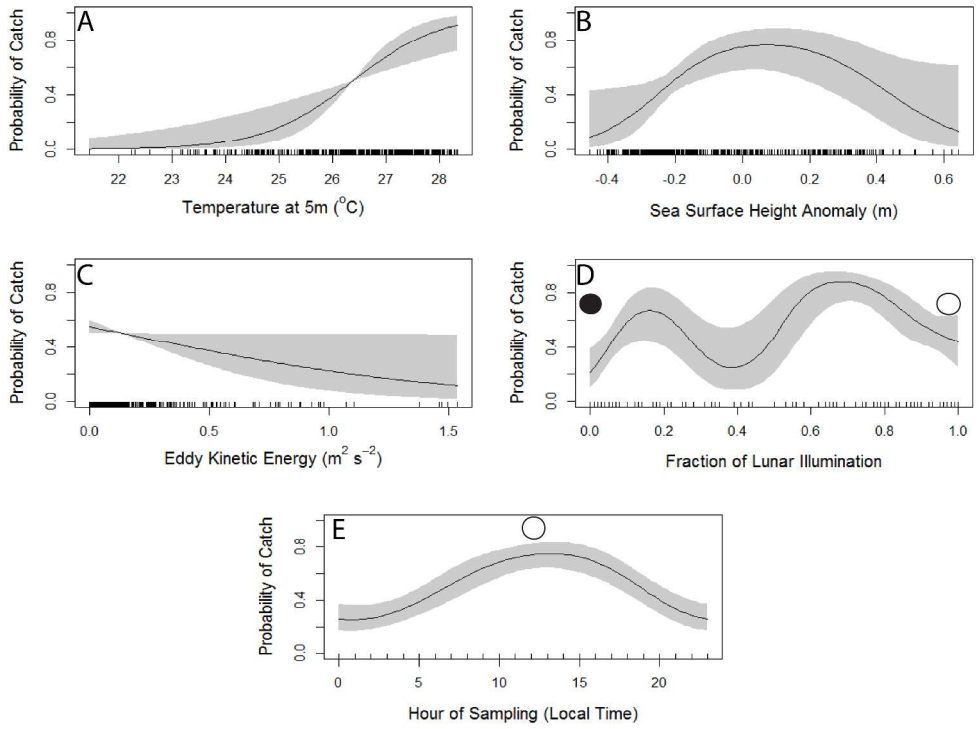

Figure 5: The response curves for a) temperature at 5m (oC), b) sea surface height anomaly (m), c) eddy kinetic energy (m2 s-2), d) fraction of lunar illumination with the dark circle indicating the new moon and the open circle representing the full moon, and e) hour of sampling, with the open circle indicating local noon.

429x341mm (300 x 300 DPI)

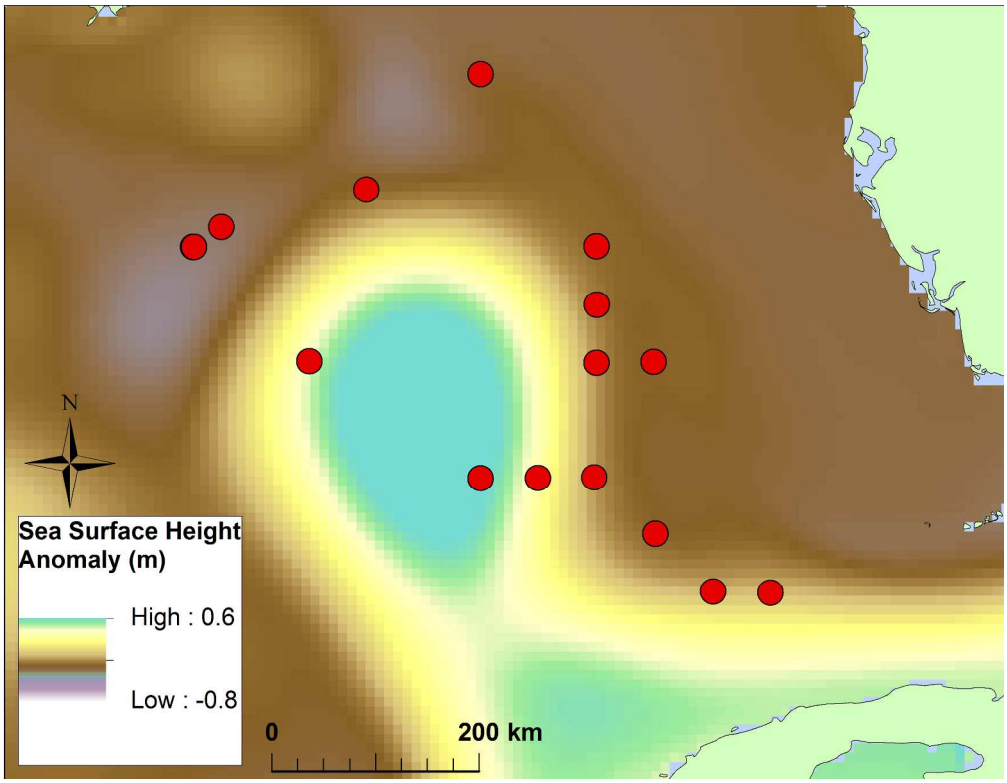

Figure 6: Catch of swordfish larvae in the Loop Current in 2012 overlaid on sea surface height anomaly (m). Red circles (●) indicate stations that showed presence of swordfish larvae.

279x215mm (300 x 300 DPI)

Supp. Table 1: Standard length, time, and location of swordfish larvae used in this study. N represents number of swordfish larvae caught by the S-10 and neuston net at each station.

Cruise	Date	Latitude	Longitude	Gear	N	Standard Length (mm)
GU1001	4/10/2010	20.7711	-86.5233	S-10	5	7.32-10.56
GU1001	4/10/2010	20.7773	-86.3936	S-10	2	4.73-6.78
GU1001	4/10/2010	20.9998	-86.6358	Neuston	1	6.66
GU1001	4/10/2010	21.0061	-86.004	S-10	3	3.54-6.31
GU1001	4/10/2010	21.0061	-86.004	Neuston	1	5.55
GU1001	4/10/2010	21.0071	-86.529	S-10	3	4-6.1
GU1001	4/11/2010	21.4841	-86.2376	S-10	1	6.01
GU1001	4/11/2010	21.4986	-85.9988	Neuston	1	8.07
GU1001	4/11/2010	21.7298	-86.2341	S-10	1	4.27
GU1001	4/11/2010	21.9985	-86.511	S-10	2	4.57-11.51
GU1001	4/12/2010	23.2012	-87.1788	S-10	1	4.3
GU1001	4/13/2010	23.4192	-87.3669	S-10	3	4.68-5.48
GU1001	4/13/2010	23.5531	-87.458	S-10	2	6.57-11.26
GU1001	4/28/2010	25.4893	-85.998	S-10	1	5.82
GU1001	4/28/2010	25.4926	-86.446	S-10	1	10.95
GU1001	4/29/2010	24.4922	-85.9979	S-10	2	3.72-25.68
GU1001	4/29/2010	24.9881	-84.9955	Neuston	1	10.05
GU1001	4/8/2010	19.994	-87.2475	S-10	3	4.77-11.28
GU1001	4/8/2010	20.0641	-87.1886	Neuston	17	2.86-6.72
GU1001	4/8/2010	20.1165	-87.0748	S-10	2	9.39-11.95
GU1001	4/8/2010	20.1693	-86.9623	S-10	5	3.55-4.4
GU1001	4/9/2010	20.2411	-86.8641	S-10	1	4.12
GU1001	4/9/2010	20.5005	-86.7161	S-10	2	3.81
GU1001	4/9/2010	20.5023	-85.8713	S-10	2	3.88-6.67
GU1001	4/9/2010	20.5105	-85.4938	S-10	2	3.64-3.89
GU1001	5/12/2010	26.0054	-87.5019	S-10	1	3.87
GU1001	5/12/2010	26.0148	-87.994	S-10	2	2.08-2.87
GU1001	5/12/2010	26.2829	-86.9944	S-10	2	2.8-3.12
GU1001	5/12/2010	26.501	-87.0005	S-10	3	3.78-4.32
GU1001	5/13/2010	26.5063	-87.9937	S-10	1	2.96
GU1001	5/22/2010	26.0029	-88.9991	S-10	1	4.11
GU1101	3/31/2011	18.8942	-78.2623	S-10	1	6.5
GU1101	4/1/2011	18.7633	-74.9499	S-10	1	3.9
GU1101	4/16/2011	16.975	-84.4886	S-10	3	4.2-5.1
GU1101	4/16/2011	17.118	-84.3708	S-10	1	6.9
GU1101	4/17/2011	16.9395	-85.2278	S-10	1	5.4
GU1101	4/19/2011	16.83	-87.0612	S-10	1	4
GU1101	4/19/2011	17.2533	-86.4111	S-10	1	6.46

Cruise	Date	Latitude	Longitude	Gear	N	Standard Length (mm)
GU1101	4/19/2011	17.2533	-86.4111	Neuston	1	6.29
GU1101	4/21/2011	18.8438	-86.8526	S-10	2	5.6-8.9
GU1101	4/21/2011	18.8438	-86.8526	Neuston	1	7.6
GU1101	4/23/2011	20.0735	-86.1522	S-10	1	6.9
GU1101	4/23/2011	20.2111	-87.1356	S-10	1	7.9
GU1101	4/24/2011	21.0748	-86.1676	Neuston	1	13
GU1101	4/25/2011	20.4113	-87.1545	S-10	1	6.25
GU1101	4/25/2011	20.4113	-87.1545	Neuston	2	3.25-8
GU1101	4/25/2011	20.4343	-87.0401	S-10	1	17.5
GU1101	4/25/2011	20.4933	-87.0773	S-10	3	6.7-11.87
GU1101	4/3/2011	17.7941	-75.4387	S-10	1	10
GU1101	4/3/2011	18.1151	-74.99	S-10	1	9.5
GU1101	4/3/2011	18.5355	-74.9028	Neuston	1	10.7
GU1101	4/5/2011	18.8322	-78.0036	S-10	1	4.8
GU1101	4/5/2011	18.9693	-77.7284	Neuston	1	3.4
GU1101	4/6/2011	18.1357	-79.8196	Neuston	1	6.2
GU1101	5/15/2011	28.009	-89.0103	S-10	1	23.1
GU1101	5/22/2011	26.5008	-90.999	S-10	1	8.37
GU1101	5/23/2011	25.9993	-89.3346	S-10	1	3.79
GU1101	5/24/2011	26.0165	-88.9946	S-10	1	3.84
GU1101	5/25/2011	25.9875	-87.498	S-10	3	4.95-8.82
GU1101	5/25/2011	26.2705	-87.0073	S-10	12	3.25-6.99
GU1101	5/25/2011	26.489	-86.9971	S-10	3	6.76-11.86
GU1101	5/25/2011	26.489	-86.9971	Neuston	1	5.32
GU1101	5/26/2011	26.9955	-86.992	S-10	12	3.44-9.32
GU1101	5/26/2011	26.9955	-86.992	Neuston	7	6.73-13.94
GU1101	5/26/2011	27.7516	-87.0018	S-10	1	9.42
GU1101	5/27/2011	28.826	-87.0031	S-10	1	6.02
GU1101	5/3/2011	23.9987	-83.4882	S-10	2	4.85-10.71
GU1101	5/4/2011	24.5111	-83.986	Neuston	1	8.09
GU1101	5/5/2011	24.9918	-85.5051	S-10	1	8.7
GU1101	5/5/2011	24.9925	-85.0026	S-10	3	6.04-13.02
GU1101	5/8/2011	27.5095	-86.994	S-10	1	4.88
GU1201	4/30/2012	24.986	-85.5063	S-10	8	4.37-9.8
GU1201	4/30/2012	24.9925	-85.0145	S-10	1	4.74
GU1201	5/1/2012	24.0006	-83.9836	S-10	1	4.07
GU1201	5/1/2012	24.5016	-84.4856	S-10	1	5.82
GU1201	5/17/2012	26.9988	-88.4993	S-10	2	2.79-3.64
GU1201	5/2/2012	23.9906	-83.4855	S-10	1	6.09
GU1201	5/22/2012	26.0206	-95.0118	S-10	1	4.87
GU1201	5/22/2012	26.0206	-95.0118	Neuston	1	4.19
GU1201	5/26/2012	26.9991	-88.4921	S-10	1	4.76

Cruise	Date	Latitude	Longitude	Gear	N	Standard Length (mm)
GU1201	5/26/2012	27.1701	-88.254	S-10	2	3.62-3.93
GU1201	5/3/2012	25.9948	-84.9971	S-10	2	4.54-7.96
GU1201	5/3/2012	26.0026	-84.5	S-10	1	8.05
GU1201	5/3/2012	26.4983	-84.9938	S-10	1	16.52
GU1201	5/3/2012	26.4983	-84.9938	Neuston	1	5.15
GU1201	5/3/2012	27.0031	-84.9968	S-10	2	7.12-7.73
GU1201	5/3/2012	27.0031	-84.9968	Neuston	1	9.59
GU1201	5/5/2012	27.506	-86.005	Neuston	1	11.44
GU1201	5/5/2012	28.5051	-86.0021	S-10	1	4.55
GU1201	5/6/2012	24.9853	-86.0033	S-10	5	3.22-5.07
GU1201	5/6/2012	24.9853	-86.0033	Neuston	1	8.9
GU1201	5/6/2012	26.0016	-86.0136	Neuston	1	12.47
GU1201	5/7/2012	26.0066	-87.4911	S-10	1	8.37
GU1201	5/9/2012	27.4965	-86.9958	S-10	1	7.69
GU1201	5/9/2012	27.4965	-86.9958	Neuston	3	5.03-6.79